

The East Greenland Polar Front as a Mediator of Climate-Ocean-Ecosystem Variability Along Southeast Greenland



Key Points:

- We present a climatology of East Greenland Polar Front intensity produced from daily sea surface temperature fields from 1993 to 2021
- The subpolar gyre drives variability in frontal intensity and impacts chlorophyll-*a* patterns with a contracted gyre boosting concentrations
- Sea-ice retreat coincides with a shoreward shift of the main front, altering the distribution of chlorophyll-*a* over the Ammassalik shelf

Supporting Information:

Supporting Information may be found in the online version of this article.

Correspondence to:

C. V. B. Gjelstrup,
cvbgj@aqu.dtu.dk

Citation:

Gjelstrup, C. V. B., Boje, J., MacKenzie, B. R., Post, S., Werner, K. M., Visser, A. W., & Stedmon, C. A. (2025). The East Greenland Polar Front as a mediator of climate-ocean-ecosystem variability along southeast Greenland. *Journal of Geophysical Research: Oceans*, 130, e2025JC022669. <https://doi.org/10.1029/2025JC022669>

Received 22 MAR 2025

Accepted 15 SEP 2025

Author Contributions:

Conceptualization: C. V. B. Gjelstrup

Data curation: J. Boje

Formal analysis: C. V. B. Gjelstrup, S. Post

Funding acquisition: C. A. Stedmon

Investigation: C. V. B. Gjelstrup, S. Post, K. M. Werner, A. W. Visser, C. A. Stedmon

Methodology: C. V. B. Gjelstrup, B. R. MacKenzie, S. Post, K. M. Werner

Supervision: C. A. Stedmon

Visualization: C. V. B. Gjelstrup

Writing – original draft:

C. V. B. Gjelstrup, S. Post

© 2025. The Author(s).

This is an open access article under the terms of the [Creative Commons Attribution License](https://creativecommons.org/licenses/by/4.0/), which permits use, distribution and reproduction in any medium, provided the original work is properly cited.

C. V. B. Gjelstrup^{1,2} , J. Boje^{1,3} , B. R. MacKenzie¹, S. Post³, K. M. Werner⁴, A. W. Visser¹ , and C. A. Stedmon¹ 

¹National Institute of Aquatic Resource, Technical University of Denmark, Lyngby, Denmark, ²Now at School of Earth and Environmental Sciences, University of St Andrews, St Andrews, UK, ³Greenland Institute of Natural Resources, Nuuk, Greenland, ⁴Thünen Institute of Sea Fisheries, Bremerhaven, Germany

Abstract The southeast Greenland region features a confluence of Arctic- and Atlantic origin waters along the continental shelf-break, forming the East Greenland Polar Front (EGPF). Here we examine the role of the EGPF in mediating climate-ocean-ecosystem variability. We observe systematic temporal variability in frontal intensity related to regional subpolar gyre (SPG) dynamics via gyre spin-up. By combining sea surface temperature derived frontal metrics with sea surface height, sea-ice concentration, surface chlorophyll-*a* concentration, and fisheries survey data, we demonstrate how gyre-induced oceanic variability is reflected in the shelf ecosystem. Elevated chlorophyll-*a* concentrations along the continental slope correspond to periods when the SPG is in a negative phase, the Irminger Gyre is spun-up and the EGPF is strong. This response in chlorophyll-*a* is likely due to a combination of aggregation of phytoplankton at the frontal zone and enhanced new production fueled by increased nutrient availability. In addition to the temporal variability, the EGPF exhibits spatial variability on seasonal and interannual timescales across the wide Ammassalik shelf. As such, the EGPF has migrated 90 km shoreward in tandem with sea-ice retreat since the early 2010s. This migration led to increased chlorophyll-*a* concentrations over shallow banks and decreased chlorophyll-*a* concentrations over the outer shelf and slope areas. Our findings underscore the critical role of the EGPF in mediating interactions between the physical and biological components of the southeast Greenland ecosystem.

Plain Language Summary The East Greenland region can be characterized as a transition zone between cold, fresh waters of Arctic origin and comparatively warm and salty waters of Atlantic origin. A strong hydrographic front, known as the East Greenland Polar Front (EGPF), separates the two domains. Frontal regions are commonly associated with elevated levels of biological productivity. This is also the case for East Greenland, where fishing efforts have historically been concentrated along the slope coincident with the EGPF. Here, we investigate the role of fluctuations in the position and intensity of the EGPF in shaping oceanographic conditions, and consequently biological productivity. We find the intensity of the EGPF is related to open-ocean gyre circulation. Sustained periods with strong gyre circulation favor a strong EGPF and enhanced surface chlorophyll concentrations along the southeast Greenland slope. In addition, we find that the EGPF migrates over the widest part of the shelf on seasonal and interannual timescales in tandem with the sea-ice cover. This migration led to a redistribution of surface chlorophyll concentrations, with increased concentrations over shallow banks and decreased concentrations over the outer shelf and slope. This work highlights the central role of EGPF in mediating climate-ocean-ecosystem variability in southeast Greenland.

1. Introduction

Fronts are some of the most ecologically important features of the ocean and often associated with high levels of biological productivity across the entire food web. This is a corollary of the influence of fronts on exchanges with the surrounding environment. Fronts impact these exchanges in two main ways: Firstly, they act as physical barriers to horizontal mixing limiting exchange of properties and materials in the across-front direction (Belkin et al., 2009). Secondly, fronts are zones of pronounced vertical exchange. This motion is facilitated by a cross-front overturning cell sustaining upwelling and subduction along the front (McWilliams, 2021). Consequently, nutrient-rich subsurface waters are brought into the surface ocean where primary producers constrained to the euphotic zone reside (Zhang et al., 2019). Surface-subsurface exchange is further catalyzed by the generation of eddies and filaments in association with fronts (Falkowski et al., 1991; Stukel et al., 2017). Elevated phytoplankton production and subsequent zooplankton grazing are therefore commonly found in association with

Writing – review & editing:

C. V. B. Gjelstrup, J. Boje,
B. R. MacKenzie, K. M. Werner,
A. W. Visser, C. A. Stedmon

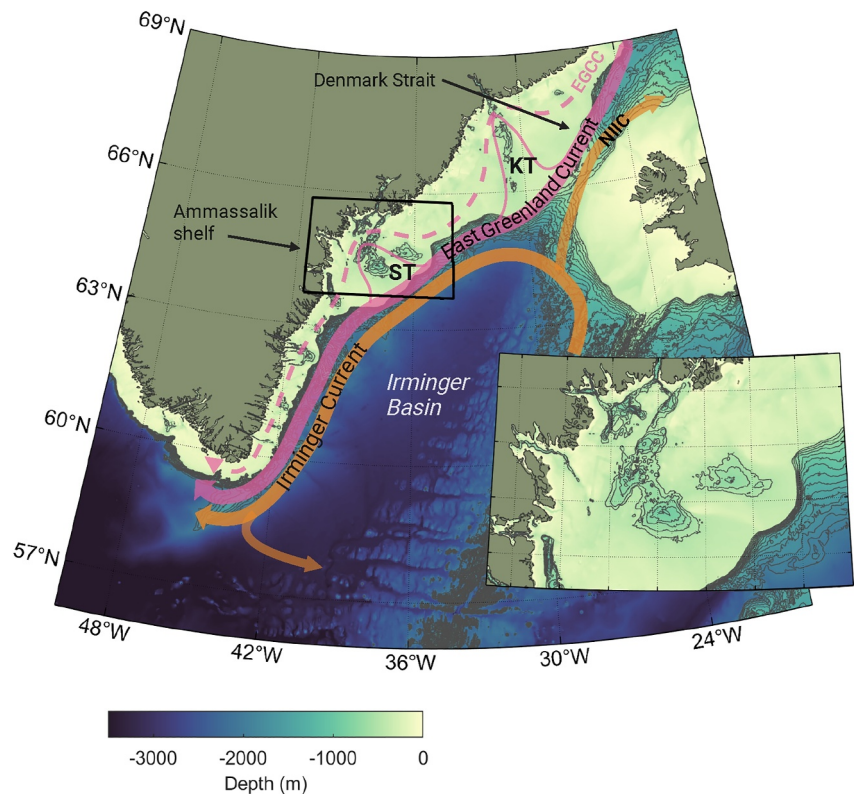


Figure 1. Schematic of major surface circulation features in southeast Greenland. Pink arrows denote cool Arctic-derived waters and orange arrows denote Atlantic origin waters. Depth contours every 100 m between 500 and 2,000 m are superimposed. The insert shows the Ammassalik shelf including Sermilik trough. EGCC: East Greenland Coastal Current, NICC: North Icelandic Irminger Current, ST: Sermilik trough, KT: Kangerlussuaq Trough.

frontal zones (Belkin et al., 2009; Chapman et al., 2020; Munk, 2014), which in turn attracts and supports pelagic and demersal fish stocks (Jansen et al., 2021). This is well known for the southeast Greenland region, where commercially valuable fish stocks, such as Greenland halibut, Atlantic cod, Atlantic mackerel, capelin, blue whiting, and redfish reside (ICES, 2024). The respective fisheries for these stocks are focused on areas along the continental shelf break region south of Denmark Strait coincident with the main frontal feature in the region—the East Greenland Polar Front (EGPF; Figure 1).

The southeast Greenland region is a transition zone between cold fresh waters of Arctic origin and warm, saline waters of Atlantic origin. The EGPF runs as a sharp persistent hydrographic front along the continental shelf break separating the two domains. West of the EGPF, Polar Waters originally formed within the Arctic Ocean, are brought southwards with the East Greenland Current (EGC; Figure 1). These waters are cool and relatively fresh. To the east, warmer and more saline waters of Atlantic origin are carried into the region by the Irminger Current (IC, Våge et al., 2011). The EGC and IC flow side by side in close proximity along the continental shelf break, imposing strong horizontal gradients in hydrographic properties further isolating shelf and oceanic waters from one another. Retroflexion at the southern tip of Greenland advects a portion of these waters back eastwards to the center of the Irminger Sea forming the cyclonic Irminger gyre (Våge et al., 2011). This gyre is embedded in the larger cyclonic subpolar gyre (SPG) extending across most of the Subpolar North Atlantic (Figure 1). Further inshore over the shelf, a fresh surface intensified jet known as the East Greenland Coastal Current (EGCC) flows southwards (Figure 1). The EGCC is similarly associated with a hydrographic front separating coastal and shelf waters (Sutherland & Pickart, 2008). The EGCC, EGC, and IC interact in the vicinity of deep troughs where complex bathymetry diverts a portion of the southward flowing EGC and IC waters over the shelf (Duyck & de Jong, 2021; Sutherland & Pickart, 2008).

Temperature variations on the southeast Greenland shelf regulate both glacial and ecological processes. Past studies have used the relative dominance of cold Arctic or warm Atlantic waters on the southeast Greenland shelf

to explain variability in the shelf ecosystem and cryosphere. For example, Post et al. (2021) found that warm-adapted fish species were more abundant when the shelf waters were warm compared to cold. This variability was attributed to changes in offshore water properties regulated by SPG dynamics. In contrast, Arctic fish abundances have abruptly declined in periods when warm Atlantic origin water protrudes onto the shelf (Emblemsvåg et al., 2022). Furthermore, glaciological studies have linked trends in the position of glacial grounding lines and glacial mass loss to variable ocean temperatures on interannual to decadal timescales (Andresen et al., 2012; Chudley et al., 2023; Inall et al., 2014; Snow et al., 2021). These studies indicate that regional climate forcing can alter hydrographic conditions in the shelf ecosystem. We hypothesize that fluctuations in the position and strength of the frontal zone between the EGC and the IC regulate the intensity and location of biological productivity in the region. We address this hypothesis by first constructing metrics of frontal position and intensity and comparing these with regional climate indices and surface chlorophyll-*a* concentrations. We then conduct an analysis to clarify the biophysical ecosystem linkages between regional oceanic forcing, frontal intensity, chlorophyll-*a* concentrations, and fish biomass. Finally, we propose that this variability can be traced to higher trophic levels on the southeast Greenland shelf.

2. Materials and Methods

2.1. Derivation of Frontal Metrics for the Southeast Greenland Region

There are numerous approaches to identify and characterize oceanographic fronts (Belkin, 2021). Here we base our frontal metrics on an analysis of sea surface temperature (SST) restricting our perspective to surface features. We use SST fields from the OSTIA reanalysis product produced by the UK Met Office (Good et al., 2020). The data set consists of daily SST images provided on a 1/20th degree grid and covering the 1993–2021 period. We opt to use SST over other properties such as sea surface salinity or sea surface height (SSH) as thermal fronts are commonly collocated with density fronts in the southeast Greenland region and SST simultaneously offers the best spatial and temporal resolutions of input data available (Duyck & de Jong, 2021). Additionally, using SST avoids potential issues with altimetry based SSH products over the shallow southeast Greenland shelf, where uncertainties are higher due to sea-ice cover and signal contamination from land (Pujol et al., 2023).

We use a gradient-based approach to identify frontal zones on individual daily SST images. Specifically, we employ the Belkin and O'Reilly Algorithm (BOA) consisting of noise reduction and edge detection (Belkin & O'Reilly, 2009). Noise reduction is achieved with a 2D contextual median filter designed to suppress random noise without blurring features. The filter is a 3×3 pixel sliding window filter that only replaces the central pixel value if it is not a maximum in the context of the surrounding 5×5 pixel window. Gradients are subsequently computed with Sobel operator to reveal sharp edges indicative of frontal features. Pixels with heavy sea-ice cover (>25%) were removed prior to analysis to avoid introducing artificial thermal gradients at the sea-ice edge.

To determine whether a given gradient magnitude is sufficient to be considered a front, we compute a histogram of all SST gradient magnitudes in the data set. Pixels with gradient magnitudes above the upper 90th percentile, corresponding to $0.8^\circ\text{C km}^{-1}$, are classified as frontal pixels. All other pixels are classified as “background”, that is, non-frontal pixels. Based hereon, seasonal and monthly frontal frequency distributions are calculated to characterize the spatial persistency of major fronts in the region.

Furthermore, a frontal intensity index is derived to analyze temporal development in the intensity of major fronts on a daily time scale. Frontal intensity is defined as the maximum SST gradient at every time step along a longitudinal transect crossing the shelf and the shelf break. To ensure the index is representative of the entire southeast Greenland shelf, we first assess spatial variability in frontal intensity over the shelf. This is achieved by computing Tuckers congruence coefficient (Tucker, 1951) as a metric of similarity for time series of frontal intensity extracted along 24 evenly spaced transects across the shelf. Comparing the frontal intensity time series for each transect with that at the southernmost transect, thus indicates the degree of similarity along the shelf.

Figure 2 shows that the temporal development of frontal intensity is virtually identical to the southernmost transect (congruence >0.95; Lorenzo-Seva & ten Berge, 2006) for much of the shelf. Exceptions to this pattern occur where the shelf widens over the Ammassalik shelf (transects 11–15) and over the northernmost part of the study region near Denmark Strait (transects 22–24). This is to be expected as hydrography near Denmark Strait is influenced by processes other than those dominant south of Iceland (Våge et al., 2013). The northernmost

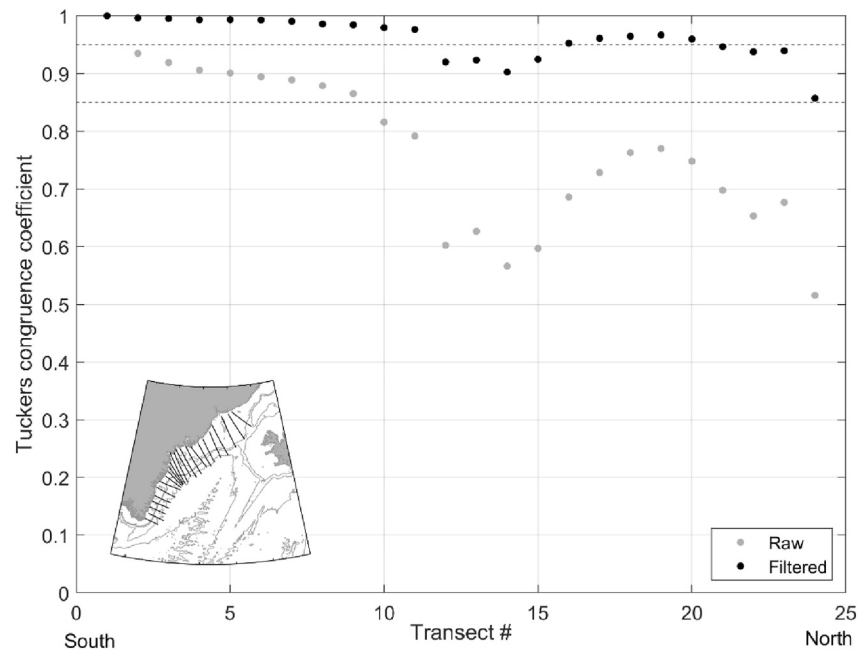


Figure 2. Tuckers congruence coefficient for time series of sea surface temperature gradients along 24 transects evenly distributed over the southeast Greenland shelf. All transects are compared with the southernmost transect (#1). Gray dots represent raw time series and black dots represent time series filtered with a 3-month moving mean filter. Transects with congruence values above 0.85 and 0.95 can be considered fairly similar and virtually identical, respectively.

transects with low congruence coefficients are therefore excluded from further analysis. The remaining transects are averaged, resulting in the shelf-wide frontal intensity index presented in Figure 3e.

2.2. Regional Climate Indices

To assess potential drivers of frontal variability, we compare our time series of derived frontal metrics with well-established regional climate indices, namely the North Atlantic Oscillation (NAO), the East Atlantic Pattern (EAP) and the SPG index. The NAO is the principal mode of sea level pressure variability in the North Atlantic. It influences North Atlantic Ocean circulation by regulating volume transport along major circulation pathways in the North Atlantic including the diversion of Atlantic origin water with the IC toward southeast Greenland (Blindheim et al., 2000; Våge et al., 2011). A high NAO index represents a strong latitudinal sea level pressure gradient between the Azores Islands and Iceland, and is associated with reduced Atlantic origin water transport with the IC toward Greenland. Conversely, a low NAO index represents a weak latitudinal sea level pressure gradient and is associated with increased IC transport (Blindheim et al., 2000; Våge et al., 2011). The EAP is the second mode of sea level pressure variability over the North Atlantic. It is associated with anomalous wind stress curl over the subpolar and subtropical gyres and is thus thought to regulate transport of subtropical origin waters into Subpolar North Atlantic (Holliday et al., 2020; Kenigson & Timmermans, 2021). A low EAP represents a large transport of subtropical origin water into the region (Häkkinen et al., 2011). Monthly time series of NAO and EAP were obtained from the National Oceanographic and Atmospheric Administration and used in statistical analyses.

The SPG index reflects semi-periodic exchange of relatively warm and light subtropical origin waters with comparatively cold and dense subpolar mode waters in the Irminger and Iceland basins (Hátún et al., 2005). This exchange effectively shifts the position of the subarctic front in the eastern North Atlantic and is often referred to as an expansion or contraction of the SPG (Kenigson & Timmermans, 2021). Many indices of SPG variability are available in the literature. These are commonly defined as a principle mode of SSH variability over the North Atlantic. Here, we extend the index presented in Hátún and Chafik (2018) to include the most recent years (2019–2021). We used monthly mean SSH fields on a $0.25^\circ \times 0.25^\circ$ grid produced by the DUACS Delayed-Time vDT2021 product and distributed by Copernicus Marine and Climate services. Following Hátún and

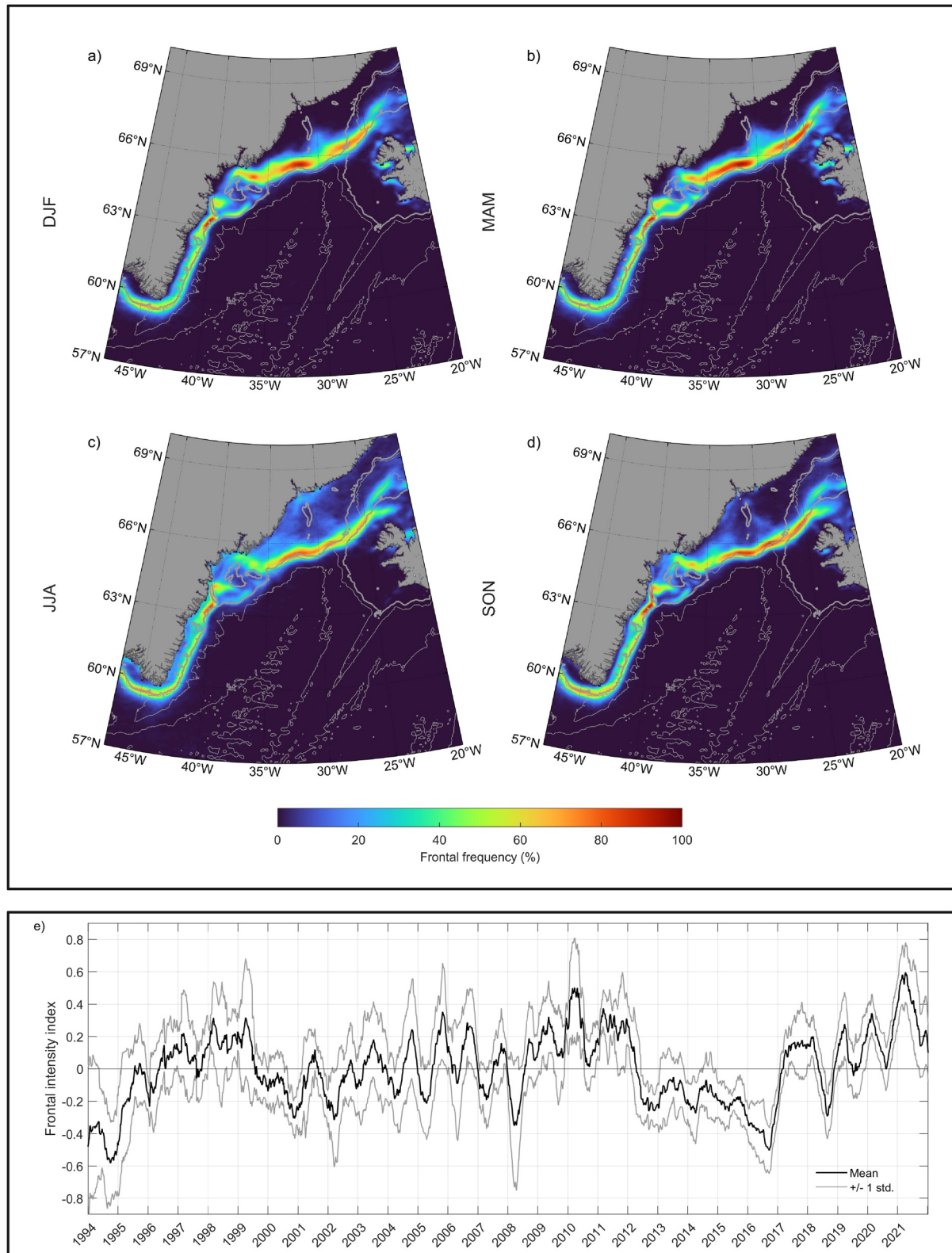


Figure 3. Frontal frequency distribution for DJF (a), MAM (b), JJA (c), and SON (d). Panel (e) shows the frontal intensity index derived from daily sea surface temperature data.

Chafik (2018), our domain covers the North Atlantic from 30°N–65°N and 80°W–0°W. Comparison between the second principle component of our Empirical Orthogonal Function analysis and the SPG index presented in Hátún and Chafik (2018) shows high degree of similarity as attested by a strong correlation coefficient of 0.90 (p -value < 0.01). The modest mismatch between our SPG index and that in Hátún and Chafik (2018) is likely due to different temporal coverage of the data sets.

2.3. Ancillary Data Sets

To aid in the interpretation of correlations between the climate indices and our frontal metrics, we compute monthly mean wind stress curl from the 10 m u - and v -components of the wind field from ERA5 produced by the European Center for Medium-Range Weather Forecasts (ECMWF; Hersbach et al., 2020). The ERA5 reanalysis product is considered reliable over the open ocean (Renfrew et al., 2021) and has been shown to agree well with a meteorological station situated in Tasiilaq in the Ammassalik region (Snow et al., 2023).

In addition, sea-ice concentration data are used to contextualize spatial variability in frontal positioning on the southeast Greenland shelf. These data are obtained from the OSTIA product at the same temporal and spatial resolutions as the SST data.

Moreover, ecological response to frontal variability is sought using remotely sensed surface chlorophyll- a concentrations. These data were obtained from the Copernicus Global Ocean Color product on a 4 × 4 km grid spanning from 1997 to 2023. Daily images were down-sampled to weekly means in order to minimize data gaps due to cloud and or sea-ice presence.

2.4. Fish Biomass Data

Survey data from the Greenlandic and German fish biomass and diversity monitoring programs in southeast Greenland are analyzed as a means to explore if oceanographic variability ripples through the food web to intermediate and higher trophic levels. For this purpose, fish catch data from 1993 to 2023 were gathered from three annual fishery-independent trawl surveys conducted in southeast Greenland, covering different regions and depths. The compiled data set includes data from 3,318 internally standardized scientific bottom trawl stations and spans the following surveys: the German groundfish survey in Greenland waters carried out by the Thünen Institute of Sea Fisheries (1993–2020; $n = 1,162$) and two Greenlandic surveys: the shrimp and fish survey (2005–2023; $n = 1,173$) and the Greenland halibut survey (1997–2023; $n = 983$), both led by the Greenland Institute of Natural Resources (Figure S1 in Supporting Information S1) (Nogueira et al., 2023; Rätz, 1996; Retzel et al., 2023). The surveys are designed to monitor groundfish species on and along the shelf and assume that catches provide a representative overview of species composition and abundance.

2.4.1. Construction of Fish Biomass Indices

The trawl survey data were used to model annual biomass indices following the approach in Post et al. (2021). Before modeling the catch data, we examined the data set for outliers, heterogeneity of variance, normality, collinearity, and independence, following the protocol outlined by Zuur et al. (2010). We identified issues with autocorrelation in latitude and longitude, so only one of these parameters was included at a time in the model. To standardize biomass and reduce bias resulting from uneven sampling effort, generalized additive models were applied (Hastie & Tibshirani, 1986). Generalized additive models are widely recognized for analyzing ecological data, including studies on fish biomass (Berg et al., 2014; Wood, 2017). This approach was particularly suitable for our study, given the presence of nonlinear relationships between observed catch data and covariates. Species occurring in fewer than 1% of all stations were excluded to avoid issues with infrequent catches. Furthermore, redfish species were omitted due to difficulties in distinguishing different species and stocks. This selection resulted in 11 species: three species typically considered polar (Greenland halibut, polar cod, and roughhead grenadier), which generally reach their southern distribution limits around southeast Greenland, and eight typically considered Atlantic species (American plaice, Atlantic cod, Atlantic wolffish, greater argentine, haddock, northern wolffish, spotted wolffish, and starry ray), which are more commonly associated with temperate waters and whose ranges extend into southeast Greenland. Thus, although the region represents a southern boundary for several of the polar species, it does not consistently represent the northern limit for all Atlantic species. Some of these species showed highly zero-inflated observations and overdispersion (with a few exceptionally large catches). To address these challenges, we employed a Tweedie distribution (Post et al., 2019; Tweedie, 1984).

Model construction was conducted using an information-theoretical approach (Burnham & Anderson, 2002). The full model assumed the following relationship for the expected biomass (μ_i) in kilograms at station i :

$$\mu_i = \text{Survey}_i + \text{Year}_i + s(\text{Swept_Area}_i) + s(\text{Lat}_i) + s(\text{Depth}_i)$$

where the expected biomass is modeled as a function of survey type and year, both treated as a factor. Swept area, latitude and depth were included as smooth functions $s()$ following the approach of Wood (2017) to account for the nonlinear effects. The final model for each species was selected using Akaike information criterion in a backward selection procedure. All analyses were performed in R (R Core Team, 2024) using the *mgcv* package (Wood, 2017). After constructing the models, we estimated annual biomass indices by predicting biomass for each year while holding the other covariates (swept area, latitude, and depth) at fixed values. Importantly, these fixed values do not affect the relative differences between years, as the year coefficients are scaled proportionally.

3. Results

3.1. Frontal Metrics

The frontal frequency distributions confirm the presence of the EGPF as the dominant frontal feature in southeast Greenland in all seasons (Figures 3a–3d and Figure S2 in Supporting Information S1). In addition, smaller transient fronts appear over the shelf during the summer months when sea-ice has retreated. The EGPF exhibits only minor variability in terms of its position. An exception to this occurs over the Ammassalik shelf, where a more complex bathymetry diverts circulation and the associated front northwards around the deep Sermilik trough (Figures 3a–3d).

Despite modest variability in the position of the front, the frontal intensity index reveals temporal fluctuations between sustained periods of high (strong SST gradients) and low (weak SST gradients) frontal intensity values (Figure 3e). The late 1990s were characterized by a strong EGPF, which decreased in intensity around 2,000 to then return to relatively high values through the mid 2000s to 2011. This prolonged period of a relatively intense EGPF was followed by a comparatively mild front between 2012 and 2016 after which the frontal intensity rapidly increased through the end of the time series (Figure 3e). Superimposed on this multiannual scale switching between high and low frontal intensities is pronounced annual variability. Frontal intensities tend to be higher during spring, indicating that the greatest contrast between the cold fresh shelf waters associated with the EGC and the comparatively warm saline waters associated with the IC is achieved at this time.

3.2. Drivers of Frontal Intensity Variability

The periodic switching between prolonged states of high and low frontal intensities alludes to possible linkages with regional climate indices. A correlation analysis between the frontal intensity index down sampled to monthly resolution and major modes of regional climate variability, found weak relations to the NAO (-0.15 , p -value <0.01) and EAP (-0.20 , p -value <0.01), and modest correspondence (-0.47 , p -value <0.01) with the SPG index (Figure 4). Frontal intensity is particularly well described by the SPG index between 1993 and 2017, as the correlation coefficient increases to -0.65 (p -value <0.01) when calculated over this period. The comparisons were evaluated at zero time lag; however, since the time series were smoothed with a 3-month moving average filter, an adjustment timescale is implicit.

Given that upper ocean currents in this region are predominantly wind-driven, it is reasonable to assume that the observed relationship between SPG variability and frontal intensity is due to advection of different source waters into the region. We test this by correlating the frontal intensity index with monthly wind stress curl. The correlations are calculated at zero lag, but the wind stress curl data were smoothed with a 3 month moving mean filter implying an adjustment timescale. Correlations did not improve when lagging the wind stress curl relative to frontal intensity. We find that the frontal intensity index is significantly correlated with wind stress curl over the central Irminger Sea with maximum correlation coefficients of 0.32 (Figure 5). This implies that an intensification of the cyclonic wind circulation over the Irminger gyre results in the appearance of stronger SST gradients, that is fronts, along the southeast Greenland slope. Whilst this relationship is statistically significant, it is relatively weak explaining a maximum of 10% of the variance. Additional processes must therefore also be influencing frontal intensity. Nevertheless, the relationship between wind stress curl and frontal intensity can be interpreted through gyre dynamics: Increased wind stress curl leads to Ekman divergence, and isopycnal heaving at the center of the

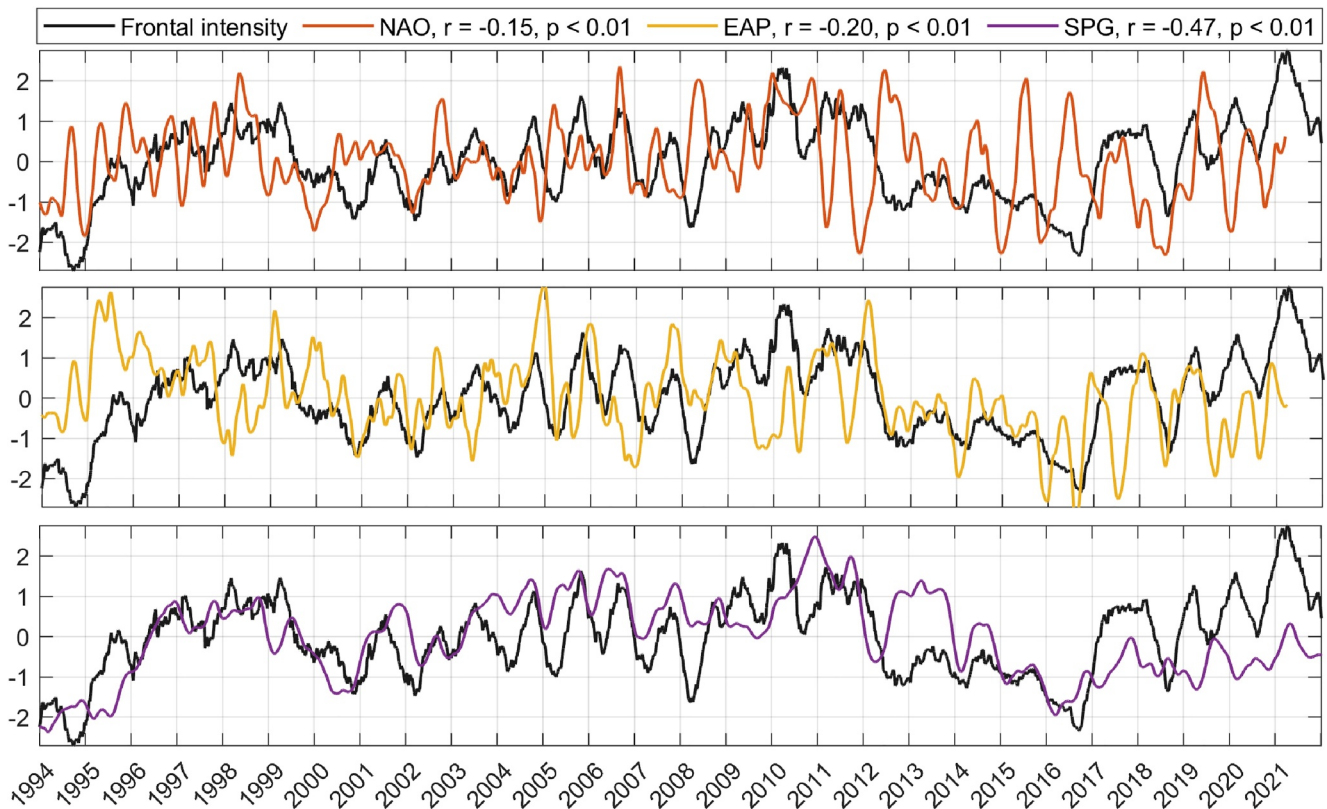


Figure 4. Comparison between the monthly frontal intensity index (black) and regional climate indices; North Atlantic Oscillation (red), East Atlantic Pattern (yellow) and Subpolar gyre (purple). Correlation coefficients and associated p-values are given in the legend. Note, all climate indices have been inverted for visualization purposes.

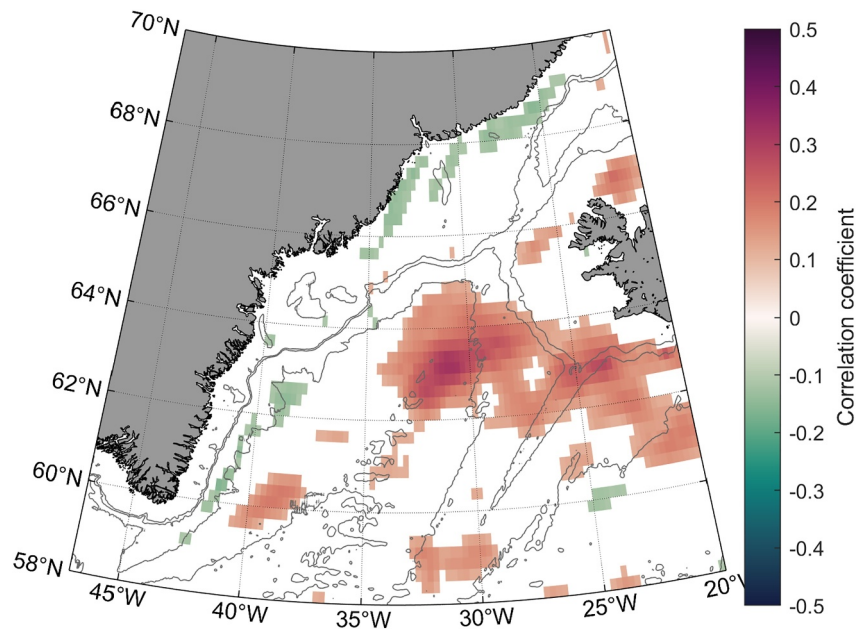


Figure 5. Correlation coefficient between the monthly frontal intensity index and wind stress curl at zero lag. Only significant (p -value < 0.05) correlations are shown. The minimum significant correlation given 28 years of monthly data availability ($N = 336$) and a p -value of 0.05 is 0.107.

gyre. Consequently, isopycnals at the gyre boundaries steepen, motivating enhanced transport of warm, saline Atlantic origin waters to the southeast Greenland slope with the IC. This in turn amplifies the temperature contrast between shelf (EGC) and basin (IC) waters which is reflected as an intensification of the front. Our interpretation is consistent with a “spin-up” of the Irminger gyre.

3.2.1. Implications of Switching SPG States on Southeast Greenland

A composite analysis of extreme SPG states is performed to explore the implications of SPG variability on the southeast Greenland shelf ecosystem. “Extreme” negative and positive SPG states are defined as the 10th and 90th quantiles of the SPG index, respectively. Composite means of the SSH, SST, horizontal SST gradient and surface chlorophyll concentration fields are shown in Figure 6. We consider the emerging patterns robust, as they are reproducible when individual extreme events are omitted.

Contrasting the SSH field during extreme SPG states reflects lowering of the sea surface during the transition from negative to positive SPG states (Figures 6a and 6b). The SPG expansion is reflected as an eastward, and slightly northward, movement of SSH contours. This transition is associated with a general cooling of the Irminger and Iceland basins as subpolar origin waters fill the basins and the warmer Atlantic origin waters are restricted eastwards (Figures 6c and 6d). Whilst this cooling trend is largely confined to the deep basins, it also affects the southeast Greenland continental slope, where the temperature contrast between shelf and oceanic waters is reduced, leading to weaker SST gradients (Figures 6e and 6f). The springtime sea-ice edge remains largely unchanged between the composite mean negative and positive SPG states, implying that the sea-ice distribution does not co-vary with SPG state (Figures 6g and 6h, black contours). This is further supported by the lack of statistically significant correlations between the SPG index and sea-ice concentrations at the shelf-break along the southeast Greenland shelf (Figure S3 in Supporting Information S1).

Surface chlorophyll-*a* concentrations indicate that phytoplankton biomass along the continental slope is influenced by SPG variability. Chlorophyll-*a* concentrations are elevated along the continental slope during extreme negative SPG states compared to the extreme positive SPG state (Figures 6g and 6h). This is attested by the statistically significant difference in annual mean chlorophyll-*a* concentrations over the slope region (between the 500 and 2,000 m isobaths). During the negative SPG state, the annual mean chlorophyll-*a* concentration is 0.64 mg m^{-3} , which reduces to 0.51 mg m^{-3} during the positive SPG state, implying a 25% increase when the SPG switches from positive to negative states on annual timescales. However, a high chlorophyll-*a* feature emerges over the outer part of the Ammassalik shelf during the positive SPG state (Figure 6h). Here, a switch from negative to positive SPG states leads to a 26% increase in surface chlorophyll-*a* concentrations on annual timescales and a 82% increase over spring. The annual development of the feature is shown on Figure S4 in Supporting Information S1.

3.2.2. Is SPG-Induced Oceanic Variability Communicated to Higher Trophic Levels?

Time series of fish biomass exhibit considerable variability, with no clear relationship to the SPG on annual timescales, as evidenced by the lack of significant correlations between the SPG index and biomass indices for any of the species (Table S1 in Supporting Information S1). Nevertheless, to examine if SPG-induced variance may be present as an underlying factor alongside other environmental factors and fisheries associated influences, we performed a Principle Component Analysis (PCA) on the species-specific biomass indices. The data were organized with the biomass indices as samples (rows) and the individual species as variables (columns). Data were mean centered and normalized prior to analysis. This identifies and isolates co-variability among the different species in the resulting scores and the associated loadings indicate how important a given principle component is for each species. The results of the PCA are presented in Figure 7.

The first principle component describes 40% of the variability in the fish biomass indices and shows a change from high to low scores over a 10-year period from 1993 to 2003, after which scores remain low and stable. The second principal component accounts for 16% of the variability in fish abundance. Its scores show distinct peaks in 1997–1998, 2004–2007, and 2022, with stable or declining periods in between. Figure 7c highlights a striking similarity between this second principal component and the SPG index. This suggests that fluctuations in the SPG influence fish biomass along southeast Greenland. The PCA decomposition furthermore demonstrates that there is no time lag between SPG changes and fish biomass responses. This suggests that the considered species have an

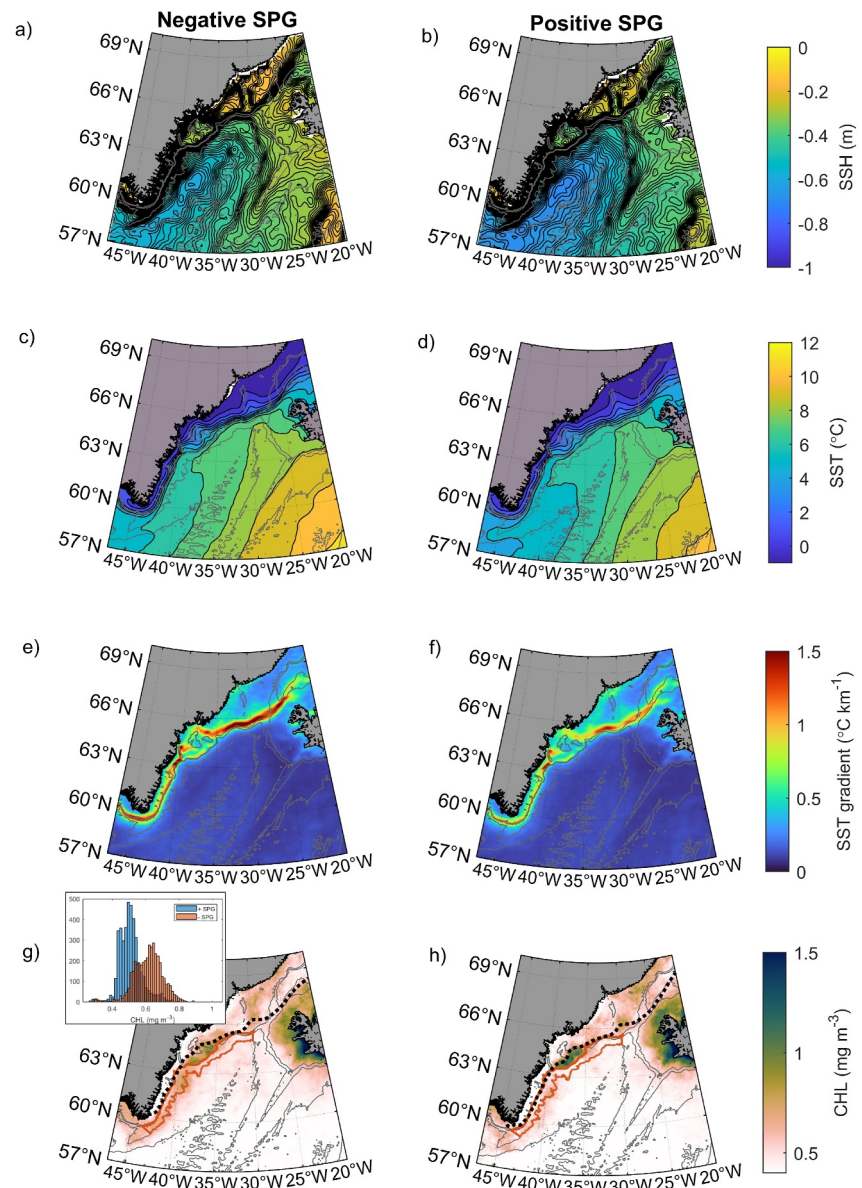


Figure 6. Composite analysis of extreme negative (left column) and positive (right column) subpolar gyre (SPG) states for sea surface height anomaly (a) and (b), sea surface temperature (SST) (c) and (d), horizontal SST gradient (e) and (f), surface chlorophyll-*a* concentrations (g) and (h), and spring (MAM) sea-ice edge (dashed black lines on g and (h)). The insert on panel (g) shows a histogram view chlorophyll-*a* concentration on the southeast Greenland slope (between the 500 and 2,000 m isobaths highlighted in orange) during extreme negative (red) and positive (blue) SPG states.

instantaneous response to the altered hydrographic conditions rather than food web interactions when analyzed at annual temporal resolution.

3.3. Sea-Ice Retreat Drives Frontal Variability on the Ammassalik Shelf

Contrary to the rest of the study region, the Ammassalik shelf experiences spatial variability in the positioning of the strongest SST front (Figures 3a–3d). There is limited spatial variability in temporal development of frontal intensity over the shelf (Figure 2), which allowed us to summarize multiple time series of frontal intensities into a singular frontal intensity index at daily resolution representative of the entire southeast Greenland shelf. However, there is reduced similarity for the wide Ammassalik shelf region indicating that additional processes are at play over this portion of the shelf. Notice this is also where the frontal zone bifurcates around the Sermilik trough

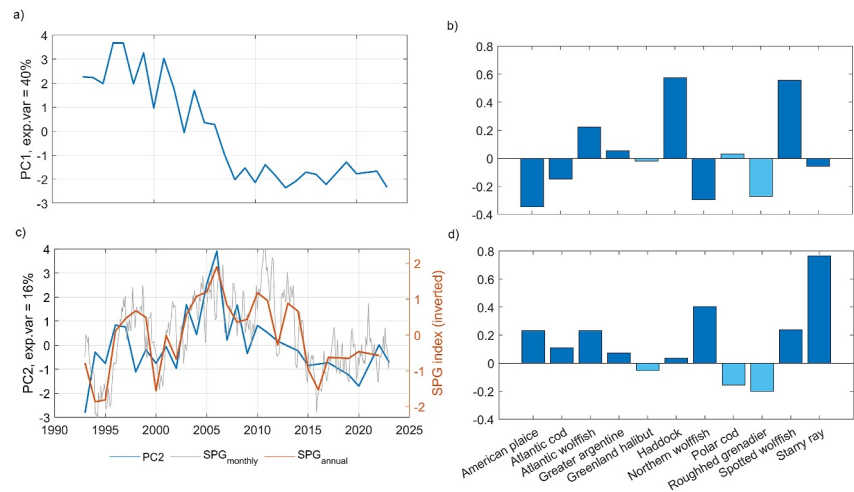


Figure 7. Principle component analysis decomposition of fisheries survey data. Panels (a and c) show the scores of the first and second principle components, respectively. Panels (b and d) give the associated loadings, where the dark and light blue shadings indicate Atlantic and polar species, respectively. The subpolar gyre index on monthly (gray) and annual (orange) timescales is superimposed on panel (c).

(Figures 3a–3d). A histogram of the frontal position along a transect crossing the Ammassalik shelf shows a clear bimodal distribution of which both modes are associated with pronounced bathymetric gradients (Figure 8a). Since the frontal intensity index represents the SST gradient at a single position at each point in time, this indicates that the strongest SST front is either located at the shelf-break or in association with the Sermilik trough. Further analysis of the spatial variability reveals a seasonal preference of the frontal route seaward around Sermilik trough during spring and shoreward of the trough during autumn (Figure 8b). Spatial coherence in the SST gradient fields suggests that this pattern is the result of a horizontal shift in the frontal positioning rather than seasonally or interannually enhanced upwelling.

In addition to seasonal variability in frontal position, Figure 8b reveals that the amplitude of this seasonal cycle is greatly reduced in recent years. The springtime position of the front during the last half of the 2010s is equivalent to the autumn position of the front in the 1993–2015 period. This shows that the seasonal migration of the front across the entire 200 km wide shelf is now reduced to approximately 70 km. Thus, there is a tendency toward a more persistent position of the front over the Ammassalik shelf.

To understand the altered seasonal cycle in the frontal position, we compare it with the position of the sea-ice edge defined as the 15% sea-ice concentration contour. The comparison is done for March, April and May since the majority of change in frontal position occurred over these months. Figure 8c shows a strong relationship between the sea-ice edge and frontal position. These results suggest that the shoreward migration of SST fronts over the

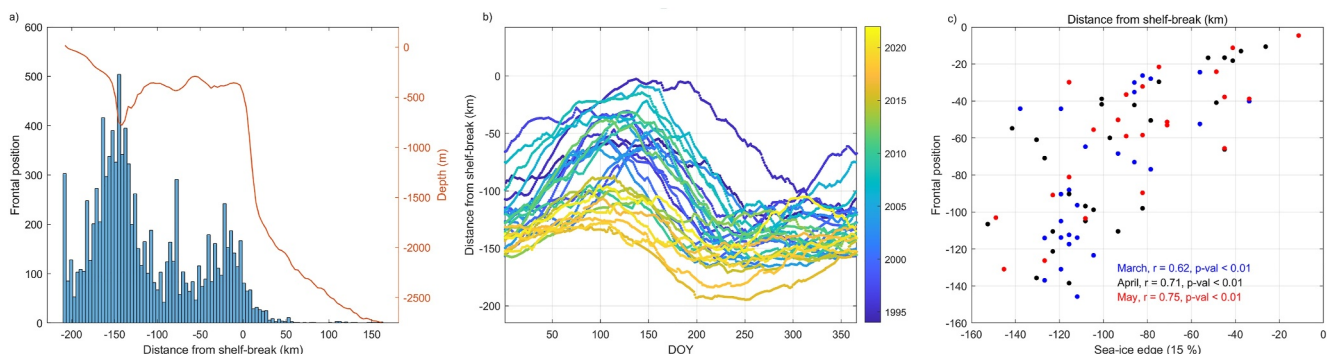


Figure 8. Frontal variability over the Ammassalik shelf. Histogram of the position of the strongest front (a), seasonal and interannual migration of frontal position (b) and comparison between the position of the sea-ice edge and the strongest front (c). Distances are negative toward the coast.

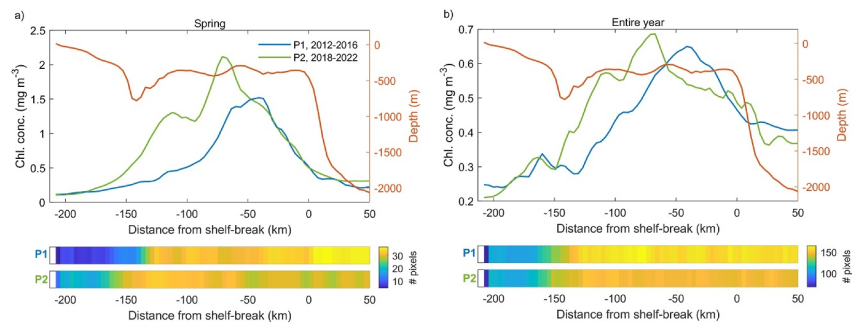


Figure 9. Surface chlorophyll-*a* concentration across the Ammassalik shelf averaged over the 2012–2016 (blue) and 2018–2022 (green) periods. Calculated for spring (days 90–140; a) and the entire year (b). The right axis shows bathymetry across the shelf. The bars below each graph show the number of cloud- and ice-free pixels available for each of the two periods. Distances are negative toward the coast.

Ammassalik shelf reflects the retreat of local sea-ice as corroborated by a strong correlation between the position of the sea-ice edge and the front (Figure 8c).

Does the shelf ecosystem respond to the pronounced change in seasonality of the frontal position? Given the influence of fronts on exchanges between the ocean, atmosphere and cryosphere, it is reasonable to assume that the uncovered frontal variability would be reflected in the shelf ecosystem. To probe this question, we consider the mean distribution of weekly surface chlorophyll-*a* concentrations across the Ammassalik shelf for the 2012–2016 and 2018–2022 periods (Figure 9). These periods were chosen as they reflect the frontal variability described above and have adequate data coverage in terms of cloud- and ice-free pixels to assess changes (Figure 9, bars below main panels). Contrasting these two periods reveals a spring production over the Sermilik trough in the 2018–2022 period, which is altogether absent in 2012–2016 (Figure 9a). Furthermore, when averaged on an annual basis, a shoreward shift in peak chlorophyll-*a* production becomes apparent (Figure 9b). Surface chlorophyll-*a* concentrations thus provide observational evidence to suggest that the distribution of surface phytoplankton biomass has shifted shoreward following the migration of fronts across the shelf. This shift is evident when ice coverage on the shelf has been low and restricted to a narrow range along the coast.

4. Discussion

The EGPF is the dominant frontal feature in the southeast Greenland region, shaped by the contrast between warm, saline off-shelf waters associated with the IC and the cold, fresh shelf waters of the EGC. The seasonal modulation of the EGC waters is reflected in the short-term fluctuations in the frontal intensity index (Figure 3e). Additional sources of variability likely include advection of upstream anomalies originating in Fram Strait and the central Arctic Ocean, as well as local modifications via processes such as sea-ice melting, surface heat fluxes, and mixing with ambient waters (de Steur et al., 2018; Gladish et al., 2015). Our correlation analysis further indicates that multidecadal variability in the SPG exerts considerable influence on the frontal intensity on the oceanic side of the EGPF. Specifically, the EGPF intensity index correlates significantly with the SPG index, with values of -0.47 for the 1993–2021 period and -0.65 for 1993–2017. These results suggest that the SPG accounts for a substantial portion of the observed variability in frontal intensity. We present a schematic interpretation of the interaction between SPG variability and the southeast Greenland slope ecosystem in Figure 10.

4.1. Hydrological and Ecological Response to SPG Variability

A positive correlation with wind stress curl over the central Irminger Sea suggests that periodic switches in the intensity of the EGPF are related to SPG dynamics via wind stress curl and spin-up of the Irminger gyre. During negative SPG states wind stress curl increases over the center of the Irminger gyre driving Ekman divergence. The sea surface consequently lowers causing the isopycnals below to heave. This steepens the isopycnals at the gyre boundaries, which in turn enhances transport of warm Atlantic origin water into the region (Figure 10, point 3). As wind stress curl over the Irminger Sea accounts for only 10% of the variance in frontal intensity when analyzed at monthly temporal resolution, other processes must also be at play. It is possible that the explained variance could be higher at different temporal resolutions or when considering lagged effects. For instance, previous studies in

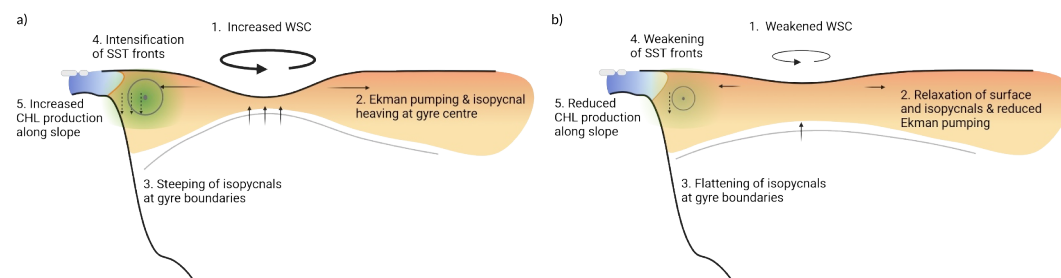


Figure 10. Schematic of interaction between subpolar gyre (SPG) variability and the southeast Greenland slope ecosystem during negative (a) and positive (b) SPG states.

the region suggest a 12–18 months time lag between wind forcing and oceanic response (Häkkinen et al., 2011; Sandø & Furevik, 2008), though we found no such evidence in our data. On the other hand, Le Bras et al. (2018) reported a strong (>0.5) positive correlation between wind forcing over the Irminger Sea and EGC/IC volume transport along the southeast Greenland slope at zero time lag using daily data, suggesting a rapid oceanic response. The timescales involved with these linkages should be further investigated in future studies. Nevertheless, the findings reported in Le Bras et al. (2018) support our interpretation of the link between wind stress curl and frontal intensity.

A composite analysis revealed significantly increased chlorophyll-*a* concentrations during the “spun-up” Irminger gyre state, that is, during times of negative SPG index and a strong EGPF. It is, however, not clear from the analysis which biophysical mechanisms are responsible for the elevated chlorophyll-*a* concentrations. Since variability in phytoplankton distribution is strongly influenced by oceanic advection, it is possible that a contribution to this signal comes from the aggregation of passive drifters (phytoplankton) at the frontal zone. In addition, differences in physical and biogeochemical conditions between positive and negative SPG states may make for more favorable phytoplankton growth conditions, and hence support more new production during the negative SPG state. Particularly relevant is the warming of ocean temperatures during the spun-up gyre state. Our composite analysis revealed a SST increase of approximately 0.75°C along the southeast Greenland shelf break, associated with a switch from a positive to negative SPG state (Figures 6c and 6d). This warming may support higher phytoplankton growth rates (Bisslinger et al., 2008; Eppley, 1972), which would contribute to the observed increase surface chlorophyll-*a* concentrations. Conversely, our analysis of sea-ice concentrations at the shelf break showed no co-variability with the SPG index (Figure S3 in Supporting Information S1), suggesting that differences in light availability due to attenuation by sea-ice is unlikely to be a significant driver of the observed differences in chlorophyll-*a* concentrations. Potential changes in light availability due to differences in mixed layer depths can, however, not be ruled out. Finally, we consider potential differences in nutrient availability. In this respect, we surmise that the effect of the spun-up state of the Irminger gyre on new production is two-fold: (a) Nutrients are more abundant due to increased (volumetric) transport of comparatively nutrient-rich waters with the IC to the slope region (Holliday et al., 2006; Le Bras et al., 2018); (b) Increased velocity of the IC causes intensification of frontal processes. Of particular relevance is strengthening of the cross-front overturning circulation cell known as the ageostrophic secondary circulation which is responsible for sustained subduction and upwelling at fronts (McWilliams, 2021). Thus, an intensification of ageostrophic secondary circulation induces enhanced vertical transport of nutrient-rich subsurface waters into the euphotic zone (Zhang et al., 2019). The combined effect is that nutrients are more readily available when the Irminger gyre is spun-up and the EGPF is strong thereby fueling phytoplankton growth and explaining the observed increase in surface chlorophyll-*a* concentrations.

The uncovered relationship between gyre variability and ecological response is opposite in sign of that along the eastern boundary of the SPG near the Iceland Basin, where a positive SPG index is associated with higher biological productivity (e.g., Hátún et al., 2016). This discrepancy is explained by the different forcing mechanisms of the ecological response. At the eastern boundary of the SPG, ecosystem impacts are primarily driven by the enhanced presence of nutrient-rich subpolar origin waters during the expanded (i.e., positive) SPG state (Hátún et al., 2016; Johnson et al., 2013). Hence, the ecosystem responds to a geometric change in the SPG. At the western boundary of the SPG in the Irminger Sea, the ecosystem impacts are rather linked to altered phytoplankton growth conditions facilitated by gyre spin-up.

A possible propagation through the food web of the SPG-induced oceanographic variability was sought through a PCA of fisheries survey data. The analysis highlights how SPG-induced oceanographic variability affects higher trophic levels with clear species-specific responses. The loadings on PC2, which reflects SPG variability, reveal that some species exhibit positive correlations, whereas others show negative correlations. This divergence aligns with the geographical distribution limits of the species. For some species, the southeast Greenland shelf represents their northernmost range, and they may benefit from increased productivity or favorable environmental conditions during a negative SPG state. For others, it marks their southernmost range, where changes such as increased temperatures or heightened competition from expanding species may create unfavorable conditions, reducing their abundance.

These findings are consistent with earlier studies, such as Núñez-Riboni et al. (2013), which demonstrated that redfish respond to SPG variability via spatial displacements, with their geographical center of mass shifting northeast-ward during a positive SPG state and south-westward during a negative SPG state. Although we did not explore redfish in this study, these results support the observed instantaneous local abundance responses of fish species on the southeast Greenland shelf to SPG variability. An immediate response of the fish community composition to temperature change was likewise noted by Emblemsvåg et al. (2022). Similarly, Post et al. (2021) emphasized that boreal species display SPG-like variability in their relative abundances, suggesting that their distributions and abundances are also influenced by hydrographic conditions shaped by the SPG.

Our analysis of the potential ecosystem and food web impacts of SPG variability and fronts along the southeast Greenland shelf does not consider intermediate trophic level species, such as zooplankton, krill or capelin. To establish more comprehensive linkages between SPG, chlorophyll-*a* concentration, and biomass of different species further studies should incorporate multiple species across trophic levels (e.g., zooplankton, benthos, and apex predators) and functional roles within the food web, as well as account for different timescales. Species specific responses to SPG-induced variability are likely to depend on specific ecological niches (e.g., trophic level) and life histories.

Profound changes in the southeast Greenland ecosystem were recently documented and related to the disappearance of summer sea-ice and warming ocean temperatures in the region (Heide-Jørgensen et al., 2023). We furthermore find the semi-periodic oceanographic variability forced by SPG fluctuations to be an additional driver of ecosystem variability in southeast Greenland. This SPG-induced oceanic variability represents a major mode of SST variability (Saes et al., 2022), so it is unsurprising that it is important for the physical oceanography of this region. Here, we additionally show that SPG variability plays a critical role in determining the frontal intensity of the EGPF. Furthermore, surface chlorophyll-*a* concentrations offer observational evidence that the surface phytoplankton biomass responds to this oceanographic variability via increased biomass over the slope region, potentially by as much as 25% during the most productive period of the year. Thus, there is emerging evidence that variability introduced by oceanic changes in light of SPG variability influence surface phytoplankton biomass which could potentially propagate through the ecosystem. Additionally, fish species with the potential for long lifespans appear to respond almost instantaneously to these changes, indicating that factors beyond phytoplankton biomass, such as shifts in species distributions or migrations into the area during certain SPG states, may also play a significant role. This highlights the complex and dynamic interactions within the ecosystem driven by SPG-induced oceanographic variability.

4.2. Sea-Ice Retreat Over the Ammassalik Shelf

Shoreward migration of SST fronts coincided with sea-ice retreat over the Ammassalik shelf. A strong correlation between the position of the springtime sea-ice edge and SST fronts implies a tight coupling between frontal positioning and the diminishing sea-ice cover. The Ammassalik shelf exhibits relatively warm surface temperatures owing to the presence of IC waters diverted onto the shelf from the main shelf-break branch of the EGC (Snow et al., 2021). This perhaps explains why sea-ice loss is particularly pronounced in this region (Gutjahr et al., 2022) and why frontal metrics here differ from the rest of southeast Greenland (Figures 2 and 3a). This suggests a positive feedback loop between sea-ice cover and frontal positioning where advection of EGC/IC waters contributes to sea-ice melt and retreat, subsequently enabling the EGC/IC diversion to extend further inshore across the shelf exacerbating sea-ice melt. A similar diversion from the main EGC branch occurs at Kangerlussuaq Trough (Figure 1). Here, complex bathymetry forces warm oceanic waters toward the coast and were found to be partially responsible for declining sea-ice cover in the vicinity of the trough (Moore et al., 2014).

An imprint of this diversion is visible from the frontal frequency distribution in Figures 3a–3d, although it is not as pronounced as at Sermilik trough.

Analysis of the surface chlorophyll-*a* distribution indicated that phytoplankton biomass responds to the frontal migration resulting in altered phytoplankton biomass patterns over the Ammassalik shelf. The shoreward migration of fronts and phytoplankton biomass are likely to become regular features of the region given that summer sea-ice is not expected to return to previous conditions (Heide-Jørgensen et al., 2023; Straneo et al., 2022). For the Ammassalik shelf, we may therefore expect a more stationary positioning of the front in the coming years. This represents a potential change in the fate of carbon with likely implications for benthic–pelagic coupling (Soltwedel et al., 2016), particularly if our surface derived patterns represent those through the water column. As such, ecosystem productivity over the shallow Ammassalik shelf could increase as sea-ice continues to retreat. The Sermilik trough currently harbors a diverse ecosystem including sponges and cold-water corals (Blicher & Hammeken Arboe, 2021). Increased anthropogenic pressures via bottom trawling, fishing, or mining activity represents a potential threat to the biodiversity of this shelf region.

5. Conclusions

By combining remotely sensed SST, SSH, sea-ice concentration, chlorophyll-*a* data, and ground fish community data we present an integrated perspective on linkages in the southeast Greenland climate-ocean-ecosystem. We show that the EGPF plays a key role in coupling oceanic and ecosystem variability and we relate changes in the positioning and intensity of this front to local sea-ice retreat and regional gyre forcing.

Although the EGPF is spatially stable along the southeast Greenland continental slope, it is temporally variable with periods of sustained high (strong) and low (weak) frontal intensity. These fluctuations reflect regional SPG dynamics via gyre spin-up bringing more and warmer Atlantic origin waters to the East Greenland slope region during negative SPG states and vice versa for positive SPG states. The resultant changes in the physical oceanography, expressed as enhancement or weakening of the intensity of the EGPF, are reflected in changes at the base of the food web. Phytoplankton biomass, proxied by surface chlorophyll-*a* concentrations, was significantly larger when the EGPF was strong, likely due to a combination of increased nutrient availability and aggregation of phytoplankton at the frontal zone. The increased chlorophyll-*a* concentrations near the frontal zone probably have consequences for productivity and distribution of species at higher trophic levels.

In addition, we show that the influence of sea-ice is most strongly felt over the relatively wide Ammassalik shelf. Here sea-ice retreat resulted in suppression of the seasonal variability in frontal position favoring a comparatively static location of the front farther inshore than previously. Altered distributions of surface chlorophyll-*a* suggest that phytoplankton biomass follows suit, trending toward increased biomass over shallow banks and reduced biomass over the outer shelf and slope regions. These changes have potential far-reaching consequences for the associated ecosystem via altered benthic–pelagic coupling and exposure of new habitats.

Conflict of Interest

The authors declare no conflicts of interest relevant to this study.

Data Availability Statement

The data used in this manuscript can be accessed via:

- OSTIA sea surface temperature and sea-ice fields, <https://doi.org/10.48670/moi-00168>. Downloaded on 17-11-2023 from: https://data.marine.copernicus.eu/product/SST_GLO_SST_L4_REP_OBSERVATIONS_010_011/description.
- NOAA's monthly NAO and EAP indices. Downloaded 26-06-2021 from: <https://www.cpc.ncep.noaa.gov/products/precip/CWlink/pna/nao.shtml> and <https://www.cpc.ncep.noaa.gov/data/teledoc/ea.shtml#:~:text=The%20EA%20pattern%20is%20structurally,lines%20of%20the%20NAO%20pattern>, respectively.
- DUACS vDT2021 sea surface height fields, <https://doi.org/10.24381/cds.4c328c78> (Copernicus Climate Change Service, Climate Data Store, 2018b). Downloaded 29-02-2024 from: <https://cds.climate.copernicus.eu/cdsapp#!/dataset/satellite-sea-level-global?tab=overview>.

- ERA5 wind fields, <https://doi.org/10.24381/cds.f17050d7> (Copernicus Climate Change Service, 2018a). Downloaded 30-08-2022 from: <https://cds.climate.copernicus.eu/cdsapp#!dataset/10.24381/cds.f17050d7?tab=overview>.
- Copernicus-GlobColour chlorophyll-*a* fields (OCEANCOLOUR_GLO_BGC_L3_MY_009_103), <https://doi.org/10.48670/moi-00280>. Downloaded 16-02-2022 from: https://data.marine.copernicus.eu/product/OCEANCOLOUR_GLO_BGC_L3_MY_009_103/description
- The derived frontal indices and fish abundance indices are available on data.dtu with the identifier <https://doi.org/10.11583/DTU.28330640>.

Acknowledgments

CAS acknowledges funding from the Independent Research Fund Denmark Grant Number 9040-00266B and the Nordic Council of Ministers AG-Fisk Grant number (209)-2020-LEGCO. SP received funding from the Nordic Council of Ministers AG-Fisk Grant number (257)-2023-Integrated Ecosystem Assessment. BRM received funding from the European Union's Horizon 2020 Research and Innovation Program under Grant agreement Number 869383 ("Ecotip") and from the Research Council Faroes under project Grant number 8013 (BlueOcean). Figures 1 and 10 were prepared using BioRender.

References

- Andresen, C. S., Straneo, F., Ribergaard, M. H., Björk, A. A., Andersen, T. J., Kuijpers, A., et al. (2012). Rapid response of helheim glacier in Greenland to climate variability over the past century. *Nature Geoscience*, 5(1), 37–41. <https://doi.org/10.1038/ngeo1349>
- Belkin, I. M. (2021). Remote sensing of ocean fronts in marine ecology and fisheries. *Remote Sensing*, 13(5), 883. <https://doi.org/10.3390/rs13050883>
- Belkin, I. M., Cornillon, P. C., & Sherman, K. (2009). Fronts in large marine ecosystems. *Progress in Oceanography*, 81(1–4), 223–236. <https://doi.org/10.1016/j.pocean.2009.04.015>
- Belkin, I. M., & O'Reilly, J. E. (2009). An algorithm for oceanic front detection in chlorophyll and SST satellite imagery. *Journal of Marine Systems*, 78(3), 319–326. <https://doi.org/10.1016/j.jmarsys.2008.11.018>
- Berg, C. W., Nielsen, A., & Kristensen, K. (2014). Evaluation of alternative age-based methods for estimating relative abundance from survey data in relation to assessment models. *Fisheries Research*, 151, 91–99. <https://doi.org/10.1016/j.fishres.2013.10.005>
- Bisslinger, J. E., Montagnes, D. J., Sharples, J., & Atkinson, D. (2008). Predicting marine phytoplankton maximum growth rates from temperature: Improving on the eppley curve using quantile regression. *Limnology & Oceanography*, 53(2), 487–493. <https://doi.org/10.4319/lo.2008.53.2.0487>
- Blicher, M. E., & Hammeken Arboe, N. (2021). Atlas of vulnerable marine ecosystem (VME) indicators observed on bottom trawl surveys in Greenland waters during 2015–2019. *Technical Report Nr. 113, Greenland Institute of Natural Resources, Greenland*.
- Blindheim, J., Borovkov, V., Hansen, B., Malmberg, S. A., Turrell, W. R., & Østerhus, S. (2000). Upper layer cooling and freshening in the Norwegian Sea in relation to atmospheric forcing. *Deep-Sea Research Part I Oceanographic Research Papers*, 47(4), 655–680. [https://doi.org/10.1016/S0967-0637\(99\)00070-9](https://doi.org/10.1016/S0967-0637(99)00070-9)
- Burnham, K. P., & Anderson, D. R. (2002). Model selection and inference: A practical information-theoretic approach. In *The journal of wildlife management* (2nd ed., Vol. 65). Springer. <https://doi.org/10.2307/3803117>
- Chapman, C. C., Lea, M. A., Meyer, A., Sallée, J. B., & Hindell, M. (2020). Defining Southern Ocean fronts and their influence on biological and physical processes in a changing climate. *Nature Climate Change*, 10(3), 209–219. <https://doi.org/10.1038/s41558-020-0705-4>
- Chudley, T. R., Howat, I. M., King, M. D., & Negrete, A. (2023). Atlantic water intrusion triggers rapid retreat and regime change at previously stable Greenland glacier. *Nature Communications*, 14(1), 2151. <https://doi.org/10.1038/s41467-023-37764-7>
- Copernicus Climate Change Service. (2018a). ERA5 monthly averaged data on single levels from 1940 to present [Dataset]. *Copernicus Climate Change Service (C3S) Climate Data Store (CDS)*. <https://doi.org/10.24381/cds.f17050d7>
- Copernicus Climate Change Service, Climate Data Store. (2018b). Sea level gridded data from satellite observations for the global ocean from 1993 to present [Dataset]. *Copernicus Climate Change Service (C3S) Climate Data Store (CDS)*. <https://doi.org/10.24381/cds.4c328c78>
- Daniault, N., Lherminier, P., & Mercier, H. (2011). Circulation and transport at the Southeast tip of Greenland. *Journal of Physical Oceanography*, 41(3), 437–457. <https://doi.org/10.1175/2010JPO4428.1>
- de Steur, L., Peralta-Ferriz, C., & Pavlova, O. (2018). Freshwater export in the East Greenland current freshens the North Atlantic. *Geophysical Research Letters*, 45(24), 13359–13366. <https://doi.org/10.1029/2018GL080207>
- Duyck, E., & de Jong, M. F. (2021). Circulation over the south-east Greenland shelf and potential for liquid freshwater export: A drifter study. *Geophysical Research Letters*, 48(5), e2020JB020886. <https://doi.org/10.1029/2020GL091948>
- Emblemsvåg, M., Werner, K. M., Núñez-Riboni, I., Frelat, R., Torp Christensen, H., Fock, H. O., & Primicerio, R. (2022). Deep demersal fish communities respond rapidly to warming in a frontal region between Arctic and Atlantic waters. *Global Change Biology*, 28(9), 2979–2990. <https://doi.org/10.1111/GCB.16113>
- Eppley, R. W. (1972). Temperature and phytoplankton growth in the sea. *Fisheries Bulletin*, 70(4), 1063–1085.
- Falkowski, P. G., Ziemann, D., Kolber, Z., & Bienfang, P. K. (1991). Role of eddy pumping in enhancing primary production in the ocean. *Nature*, 352(6330), 55–58. <https://doi.org/10.1038/352055a0>
- Gladish, C. V., Holland, D. M., & Lee, C. M. (2015). Oceanic boundary conditions for Jakobshavn Glacier. Part II: Provenance and sources of variability of disko Bay and illulisat icefjord waters, 1990–2011. *Journal of Physical Oceanography*, 45(1), 33–63. <https://doi.org/10.1175/JPO-D-14-0045.1>
- Global Ocean Colour (Copernicus-GlobColour), Bio-Geo-Chemical, L3 (daily) from Satellite Observations (1997-ongoing). (2014). Global ocean colour (Copernicus-GlobColour), bio-geo-chemical, L3 (Daily) from Satellite Observations (1997-ongoing) [dataset]. In *E.U. copernicus marine service information (CMEMS)*. Marine Data Store (MDS). <https://doi.org/10.48670/moi-00280>
- Global Ocean OSTIA Sea Surface Temperature and Sea Ice Reprocessed. E.U. Copernicus Marine Service Information (CMEMS). (2025). Global Ocean OSTIA Sea surface temperature and sea ice reprocessed. E.U. copernicus marine service information (CMEMS) [dataset]. *Marine Data Store (MDS)*. <https://doi.org/10.48670/moi-00168>
- Good, S., Fiedler, E., Mao, C., Martin, M. J., Maycock, A., Reid, R., et al. (2020). The current configuration of the OSTIA system for operational production of foundation sea surface temperature and ice concentration analyses. *Remote Sensing*, 12(4), 720. <https://doi.org/10.3390/rs12040720>
- Gutjahr, O., Jungclauss, J. H., Brüggemann, N., Haak, H., & Marotzke, J. (2022). Air-Sea interactions and water mass transformation during a katabatic storm in the Irminger Sea. *Journal of Geophysical Research: Oceans*, 127(5), e2021JC018075. <https://doi.org/10.1029/2021JC018075>
- Häkkinen, S., Rhines, P. B., & Worthen, D. L. (2011). Warm and saline events embedded in the meridional circulation of the northern North Atlantic. *Journal of Geophysical Research*, 116(3), C03006. <https://doi.org/10.1029/2010JC006275>
- Hastie, T., & Tibshirani, R. (1986). Generalized additive models. *Statistical Science*, 1(3), 297–310. <https://doi.org/10.1214/ss/1177013604>

- Hátún, H., & Chafik, L. (2018). On the recent ambiguity of the North Atlantic subpolar gyre index. *Journal of Geophysical Research: Oceans*, 123(8), 5072–5076. <https://doi.org/10.1029/2018JC014101>
- Hátún, H., Lohmann, K., Matei, D., Jungclauss, J. H., Pacariz, S., Bersch, M., et al. (2016). An inflated subpolar gyre blows life toward the northeastern Atlantic. *Progress in Oceanography*, 147, 49–66. <https://doi.org/10.1016/j.POCEAN.2016.07.009>
- Hátún, H., Sande, A. B., Drange, H., Hansen, B., & Valdimarsson, H. (2005). Influence of the Atlantic subpolar gyre on the thermohaline circulation. *Science*, 309(5742), 1841–1844. <https://doi.org/10.1126/science.1114777>
- Heide-Jørgensen, M. P., Chambault, P., Jansen, T., Gjelstrup, C. V. B., Rosing-Asvid, A., Macrander, A., et al. (2023). A regime shift in the Southeast Greenland marine ecosystem. *Global Change Biology*, 29(3), 668–685. <https://doi.org/10.1111/gcb.16494>
- Hersbach, H., Bell, B., Berrisford, P., Hirahara, S., Horányi, A., Muñoz-Sabater, J., et al. (2020). The ERA5 global reanalysis. *Quarterly Journal of the Royal Meteorological Society*, 146(730), 1999–2049. <https://doi.org/10.1002/qj.3803>
- Holliday, N. P., Bersch, M., Brix, B., Chafik, L., Cunningham, S., Florindo-López, C., et al. (2020). Ocean circulation causes the largest freshening event for 120 years in eastern subpolar North Atlantic. *Nature Communications*, 11(1), 585. <https://doi.org/10.1038/s41467-020-14474-y>
- Holliday, N. P., Waniek, J. J., Davidson, R., Wilson, D., Brown, L., Sanders, R., et al. (2006). Large-scale physical controls on phytoplankton growth in the Irminger Sea Part I: Hydrographic zones, mixing and stratification. *Journal of Marine Systems*, 59(3–4), 201–218. <https://doi.org/10.1016/j.jmarsys.2005.10.004>
- ICES. (2024). Greenland Sea ecoregion – Fisheries overview. In *Report of the ICES Advisory Committee, 2024, section 10.2*. <https://doi.org/10.17895/ices.advice.27879759>
- Inall, M. E., Murray, T., Cottier, F. R., Scharrer, K., Boyd, T. J., Heywood, K. J., & Bevan, S. L. (2014). Oceanic heat delivery via Kangerdlugssuaq Fjord to the south-east Greenland ice sheet. *Journal of Geophysical Research: Oceans*, 119(2), 631–645. <https://doi.org/10.1002/2013JC009295>
- Jansen, T., Nielsen, E. E., Rodriguez-Ezpeleta, N., Arrizabalaga, H., Post, S., & Mackenzie, B. R. (2021). Atlantic bluefin tuna (*Thunnus thynnus*) in Greenland—Mixed-stock origin, diet, hydrographic conditions, and repeated catches in this new fringe area. *Canadian Journal of Fisheries and Aquatic Sciences*, 78(4), 400–408. <https://doi.org/10.1139/cjfas-2020-0156>
- Johnson, C., Inall, M., & Häkkinen, S. (2013). Declining nutrient concentrations in the northeast Atlantic as a result of a weakening Subpolar Gyre. *Deep-Sea Research Part I: Oceanographic Research Papers*, 82, 95–107. <https://doi.org/10.1016/j.dsr.2013.08.007>
- Kenigson, J. S., & Timmermans, M. L. (2021). Nordic seas hydrography in the context of arctic and north Atlantic ocean dynamics. *Journal of Physical Oceanography*, 51(1), 101–114. <https://doi.org/10.1175/JPO-D-20-0071.1>
- Le Bras, I. A. A., Straneo, F., Holte, J., & Holliday, N. P. (2018). Seasonality of Freshwater in the East Greenland Current System from 2014 to 2016. *Journal of Geophysical Research: Oceans*, 123(12), 8828–8848. <https://doi.org/10.1029/2018JC014511>
- Lorenzo-Seva, U., & ten Berge, J. M. F. (2006). Tucker's congruence coefficient as a meaningful index of factor similarity. *Methodology*, 2(2), 57–64. <https://doi.org/10.1027/1614-2241.2.2.57>
- McWilliams, J. C. (2021). Oceanic frontogenesis. *Annual Review of Marine Science*, 13(1), 227–253. <https://doi.org/10.1146/annurev-marine-032320-120725>
- Moore, G. W. K., Straneo, F., & Oltmanns, M. (2014). Trend and interannual variability in southeast Greenland Sea Ice: Impacts on coastal Greenland climate variability. *Geophysical Research Letters*, 41(23), 8619–8626. <https://doi.org/10.1002/2014GL062107>
- Munk, P. (2014). Fish larvae at fronts: Horizontal and vertical distributions of gadoid fish larvae across a frontal zone at the Norwegian Trench. *Deep-Sea Research Part II: Topical Studies in Oceanography*, 107, 3–14. <https://doi.org/10.1016/j.dsr2.2014.01.016>
- Nogueira, A., Christiansen, H., & Boje, J. (2023). Survey for Greenland halibut in ICES 14b, September–October 2022. In *ICES Working Document WD07*. ICES North, 24–28 May.
- Núñez-Riboni, I., Kristinsson, K., Bernreuther, M., van Aken, H. M., Stransky, C., Cisewski, B., & Rolskiy, A. (2013). Impact of interannual changes of large scale circulation and hydrography on the spatial distribution of beaked redfish (*Sebastes mentella*) in the Irminger Sea. *Deep Sea Research Part I: Oceanographic Research Papers*, 82, 80–94. <https://doi.org/10.1016/j.dsr.2013.08.003>
- Post, S., Fock, H. O., & Jansen, T. (2019). Blue whiting distribution and migration in Greenland waters. *Fisheries Research*, 212, 123–135. <https://doi.org/10.1016/j.fishres.2018.12.007>
- Post, S., Werner, K. M., Núñez-Riboni, I., Chafik, L., Hátún, H., & Jansen, T. (2021). Subpolar gyre and temperature drive boreal fish abundance in Greenland waters. *Fish and Fisheries*, 22(1), 161–174. <https://doi.org/10.1111/faf.12512>
- Pujol, M. I., Dupuy, S., Vergara, O., Sánchez Román, A., Faugère, Y., Prandi, P., et al. (2023). Refining the resolution of DUACS along-track Level-3 Sea level altimetry products. *Remote Sensing*, 15(3), 793. <https://doi.org/10.3390/rs15030793>
- Rätz, H. J. (1996). Efficiency of geographical and depth stratification in error reduction of groundfish survey results: Case study Atlantic cod off Greenland. *NAFO Scientific Council Studies*, 28, 65–71.
- R Core Team. (2024). A Language and environment for statistical computing. In *R foundation for statistical computing* (Vol. 3). R Foundation for Statistical Computing. Retrieved from <http://www.r-project.org>
- Renfrew, I. A., Barrell, C., Elvidge, A. D., Brooke, J. K., Duschka, C., King, J. C., et al. (2021). An evaluation of surface meteorology and fluxes over the Iceland and Greenland Seas in ERA5 reanalysis: The impact of sea ice distribution. *Quarterly Journal of the Royal Meteorological Society*, 147(734), 691–712. <https://doi.org/10.1002/qj.3941>
- Retzel, A., Post, S., & Werner, K.-M. (2023). Compilation of Commercial and Survey data for the GAM, INLA, and SAM models. In *WD05 In: ICES. 2023. Benchmark workshop on Greenland cod stocks (WKBGREENCOD)*. ICES Scientific Reports. <https://doi.org/10.17895/ices.pub.22683151>
- Saes, M. J. M., Gjelstrup, C. V. B., Visser, A. W., & Stedmon, C. A. (2022). Separating annual, interannual and regional change in Sea surface temperature in the Northeastern Atlantic and Nordic Seas. *Journal of Geophysical Research: Oceans*, 127(8), e2022JC018630. <https://doi.org/10.1029/2022JC018630>
- Sandø, A. B., & Furevik, T. (2008). Relation between the wind stress curl in the North Atlantic and the Atlantic inflow to the Nordic Seas. *Journal of Geophysical Research*, 113(6), C06028. <https://doi.org/10.1029/2007JC004236>
- Snow, T., Straneo, F., Holte, J., Grigsby, S., Abdalati, W., & Scambos, T. (2021). More than skin deep: Sea surface temperature as a means of inferring Atlantic Water variability on the southeast Greenland continental shelf near Helheim Glacier. *Journal of Geophysical Research: Oceans*, 126(4), e2020JC016509. <https://doi.org/10.1029/2020jc016509>
- Snow, T., Zhnag, W., Schreiber, E., Siegfried, M., Abdalati, W., & Scambos, T. (2023). Alongshore wind-driven coastal upwelling drives Atlantic water intrusions onto the continental shelf along Sermilik Trough. *Journal of Geophysical Research: Oceans*, 128(9), e2023JC019953. <https://doi.org/10.1029/2023JC019953>

- Soltwedel, T., Bauerfeind, E., Bergmann, M., Bracher, A., Budaeva, N., Busch, K., et al. (2016). Natural variability or anthropogenically-induced variation? Insights from 15 years of multidisciplinary observations at the arctic marine LTER site HAUSGARTEN. *Ecological Indicators*, *65*, 89–102. <https://doi.org/10.1016/j.ecolind.2015.10.001>
- Straneo, F., Slater, D. A., Bouchard, C., Cape, M. R., Carey, M., Ciannelli, L., et al. (2022). An interdisciplinary perspective on Greenland's changing coastal margins. *Oceanography*, *35*(3–4), 106–117. <https://doi.org/10.5670/oceanog.2022.128>
- Stukel, M. R., Aluwihare, L. I., Barbeau, K. A., Chekalyuk, A. M., Goericke, R., Miller, A. J., et al. (2017). Mesoscale ocean fronts enhance carbon export due to gravitational sinking and subduction. *Proceedings of the National Academy of Sciences of the United States of America*, *114*(6), 1252–1257. <https://doi.org/10.1073/pnas.1609435114>
- Sutherland, D. A., & Pickart, R. S. (2008). The East Greenland Coastal Current: Structure, variability, and forcing. *Progress in Oceanography*, *78*(1), 58–77. <https://doi.org/10.1016/j.pocean.2007.09.006>
- Tucker, L. R. (1951). A method for synthesis of factor analysis studies. In *Personnel research section report* (Vol. 984).
- Tweedie, M. C. K. (1984). An index which distinguishes between some important exponential families. In *statistics: Applications and New Directions. In Proceedings of the Indian statistical Institute Golden Jubilee International conference* (Vol. 579, pp. 579–604).
- Våge, K., Pickart, R. S., Sarafanov, A., Knutsen, Ø., Mercier, H., Lherminier, P., et al. (2011). The Irminger Gyre: Circulation, convection, and interannual variability. *Deep-Sea Research Part I Oceanographic Research Papers*, *58*(5), 590–614. <https://doi.org/10.1016/j.dsr.2011.03.001>
- Våge, K., Pickart, R. S., Spall, M. A., Moore, G. W. K., Valdimarsson, H., Torres, D. J., et al. (2013). Revised circulation scheme north of the Denmark Strait. *Deep-Sea Research Part I Oceanographic Research Papers*, *79*, 20–39. <https://doi.org/10.1016/j.dsr.2013.05.007>
- Wood, S. N. (2017). Generalized additive models: An introduction with R. In C. and Hall/CRC. In *Generalized additive models: An introduction with R* (2nd ed.). <https://doi.org/10.1201/9781420010404>
- Zhang, Z., Qiu, B., Klein, P., & Travis, S. (2019). The influence of geostrophic strain on Oceanic ageostrophic motion and surface chlorophyll. *Nature Communications*, *10*(1), 2838. <https://doi.org/10.1038/s41467-019-10883-w>
- Zuur, A. F., Ieno, E. N., & Elphick, C. S. (2010). A protocol for data exploration to avoid common statistical problems. *Methods in Ecology and Evolution*, *1*(1), 3–14. <https://doi.org/10.1111/j.2041-210X.2009.00001.x>